



Published in final edited form as:

*Cancer Res.* 2009 November 15; 69(22): 8790–8796. doi:10.1158/0008-5472.CAN-08-4340.

## Intraoperative Evaluation of Breast Tumor Margins with Optical Coherence Tomography

Freddy T. Nguyen<sup>1,2,4</sup>, Adam M. Zysk<sup>3,4</sup>, Eric J. Chaney<sup>4</sup>, Jan G. Kotynek<sup>5,7</sup>, Uretz J. Oliphant<sup>5,7</sup>, Frank J. Bellafiore<sup>5,7</sup>, Kendrith M. Rowland<sup>5,7</sup>, Patricia A. Johnson<sup>5,7</sup>, and Stephen A. Boppart<sup>2,3,4,5,6,7,\*</sup>

<sup>1</sup>Department of Chemistry, University of Illinois at Urbana-Champaign 405 North Mathews Avenue Urbana, IL 61801

<sup>2</sup>College of Medicine, University of Illinois at Urbana-Champaign 405 North Mathews Avenue Urbana, IL 61801

<sup>3</sup>Department of Electrical and Computer Engineering, University of Illinois at Urbana-Champaign 405 North Mathews Avenue Urbana, IL 61801

<sup>4</sup>Beckman Institute for Advanced Science & Technology, University of Illinois at Urbana-Champaign 405 North Mathews Avenue Urbana, IL 61801

<sup>5</sup>Mills Breast Cancer Institute, 611 West Park Street Urbana, IL 61801

<sup>6</sup>Carle Foundation Hospital, 611 West Park Street Urbana, IL 61801

<sup>7</sup>Carle Clinic Association, 611 West Park Street Urbana, IL 61801

### Abstract

As breast cancer screening rates increase, smaller and more numerous lesions are being identified earlier, leading to more breast-conserving surgical procedures. Achieving a clean surgical margin represents a technical challenge with important clinical implications. Optical coherence tomography (OCT) is introduced as an intraoperative high-resolution imaging technique that assesses surgical breast tumor margins by providing real-time microscopic images up to 2 mm beneath the tissue surface. In a study of 37 patients split between training and study groups, OCT images covering 1 cm<sup>2</sup> regions were acquired from surgical margins of lumpectomy specimens, registered with ink, and correlated with corresponding histological sections. A 17 patient training set used to establish standard imaging protocols and OCT evaluation criteria demonstrated that areas of higher scattering tissue with a heterogeneous pattern were indicative of tumor cells and tumor tissue, in contrast to lower scattering adipocytes found in normal breast tissue. The remaining 20 patients were enrolled into the feasibility study. Of these lumpectomy specimens, 11 were identified with a positive or close surgical margin and 9 were identified with a negative margin under OCT. Based on histological findings, 9 true positives, 9 true negatives, 2 false positives, and 0 false negatives were found, yielding a sensitivity of 100% and specificity of 82%. These results demonstrate the potential of OCT as a real-time method for intraoperative margin assessment in breast conserving surgeries.

### Keywords

Breast Cancer; Imaging; Margin Status; Optical Coherence Tomography

---

\*boppart@illinois.edu.

## Introduction

### Breast Cancer

Improved breast cancer screening has resulted in smaller lesions being detected earlier. An estimated 192,370 new cases of invasive breast cancer (26% of newly diagnosed cancer cases in women), 62,280 new cases of ductal carcinoma *in-situ* (DCIS), and 40,610 breast cancer deaths will be reported in the United States during 2009, making it the most widely diagnosed cancer and the second leading cause of cancer deaths among women (1). Increased five-year survival rates have been attributed to increased awareness, earlier detection, and improved treatment and management. A large portion of patients undergo surgical removal of lesions via breast-conserving surgery (lumpectomy) with irradiation often accompanied by sentinel or axillary lymph node dissection for disease staging.

### Tumor Margin Assessment and Local Recurrence

As lumpectomy rates have increased over time, the definition of a clean margin has changed. A recent study reported 45.9% of radiation oncologists defined negative margins as no cancer cells at inked margins, whereas 7.4% defined it as no cells within 1 mm, and 21.8% believed it to be no cells within 2 mm (2). As more studies correlated the width of uninvolved margins to local recurrence (3,4), a more aggressive approach towards breast conservation has allowed surgeons to use 2 mm, or even 1 mm, to define a clean margin. The same survey of radiation oncologists reported that 31% of respondents defined a close margin as having no cells within 1 mm, and an additional 38% defined it to be no cells within 2 mm of the inked surface (2).

Despite this ongoing debate, the key predictor of local recurrence is the margin status (5-16). . A positive margin, the presence of disease on the inked surface, occurs in at least 30-35% of cases, and an additional 10-15% are classified as close margins (< 2 mm)(15). Local recurrence rates for breast conserving therapy followed by radiation were reported in 2-28% of cases with positive margins, 2-16% with close margins (<2 mm), and 2-8% with negative margins (15) which would be higher in the absence of radiation therapy (6,8,17,18).

### Intraoperative Margin Assessment

Currently, no real-time non-destructive intraoperative method exists to rapidly assess the microscopic status of lumpectomy margins as standard of care (19,20). Several techniques have been investigated including frozen section analysis (FSA), touch prep cytology, radiography, radiofrequency (RF) spectroscopy, and Raman spectroscopy. FSA was reported to have a sensitivity of 73.08% and a specificity of 98.32% compared to paraffin section analysis (PSA) in breast cancer (19). FSA has not widely been accepted as part of standard of care due to difficulties in performing frozen sections on adipose tissue, added time (~20-30 minutes), increased operating room time, and additional pathology evaluation with increased costs. The most significant disadvantage is the inability for FSA to be performed over the entire surface area of the tissue specimen, sharing the same sampling rate limitation as PSA in sampling only 10-15% of the surface area (21).

Touch prep cytology can rapidly assess the entire surface area, addressing the sampling rate issue while preserving the integrity of the specimen, and making it a promising technique for identifying positive margins. This technique reported sensitivities of 75% and specificities of 82.8% (21). The major disadvantages include the need for tumor cells at the surface, and their detachment. Touch prep cytology does not provide information about the presence of cancer cells beneath the surface and therefore is unable to determine close and negative margins.

Intraoperative radiography of specimens provides surgeons the ability to visualize the margin in depth by displaying two-dimensional x-ray projections. However, the low reported

sensitivity and specificity of 49% and 73%, respectively (22), are primarily due to the inability to identify diffuse microscopic processes, especially where the tumor boundary is poorly-defined (23).

RF spectroscopy provides a bulk measurement over a circular area (diameter = 0.7 cm) and within a 100  $\mu\text{m}$  depth (24). With low sensitivity (71%) and specificity (68%) (24), shallow penetration depth, and low resolution, detection within 1-2 mm for margin classification is limited. Raman spectroscopy, which extracts chemical information, was reported to have a sensitivity of 100%, a specificity of 100%, and overall accuracy of 93% in identifying carcinomas (25). Despite high sensitivity and specificity, this technique may have limited clinical utility due to point measurements with long 1 s acquisition times per point, making it unable to quickly sample large surface areas.

### Optical Coherence Tomography in Breast Cancer

Optical coherence tomography (OCT) is a high resolution microscopic optical imaging technique that yields real-time multi-dimensional images of subsurface tissue structure (26-32). OCT is the optical analogue to ultrasound imaging but uses light waves instead of sound waves to create images. Near-infrared light enables micron-scale resolution, providing images on the same resolution scale as histopathology. The penetration depth in breast tissue is approximately 1-2 mm, making OCT a suitable technology for intraoperative tumor margin assessment. The density of cells and sub-cellular scatterers (nuclei, organelles) primarily determines the depth to which the OCT light penetrates tissue and scatters back to be detected. Tissue comprised primarily of adipocytes can be imaged to depths of 2 mm, compared to 200-1000  $\mu\text{m}$  in cell-dense tumor tissue. These depths are comparable to the currently accepted margin widths that classify positive, close, and negative margins. By enabling surgeons to rapidly visualize tissue morphology beneath the surface and over large surface areas while preserving tissue structure, OCT has the potential to become an invaluable intraoperative tool for assessing margin status.

Since its introduction, OCT has capitalized on advances in telecommunications, resulting in significant increases in data acquisition speeds (33), added functional modalities (34-36), and new contrast agents (37,38). OCT has found clinical applications in ophthalmology, cardiology, gastroenterology, and oncology (39). OCT has been used to image tumor margins in an NMU-carcinogen-induced rat mammary tumor model, differentiating between highly scattering cancer cells and the fibrous / fatty tissue associated with normal mammary tissue (29,40). Increased scattering in tumor is attributed to the increase in nuclear-to-cytoplasm (N/C) ratio and the increase in cellular and nuclear density (41,42). The large size and low-scattering of adipocytes, relative to higher-scattering stromal and tumor cells, provides one method for differentiating these tissue types (29,40,43).

Access to deep breast lesions can be performed using needle-based OCT probes (43-45). These needle-probes can provide real-time information for guided lesion biopsy or for placement of localization wires (44,45). Reports identified diagnostically-significant information within the optical backscattering and refractive index signals which can distinguish various breast tissue types (29,40,46). These same diagnostic properties can be extracted from individual axial scans that comprise an OCT image, or from spatial information provided by the OCT image itself (40,45,46). This study focuses on the first intraoperative OCT assessment of exposed tumor margins.

## Materials and Methods

### Instrument

A clinical spectral-domain OCT (SD-OCT) system (Figures 1 & 2) was constructed to assess surgical margins from lumpectomy specimens. The OCT system employs a super-luminescent diode (SLD) (Model SLD1C, B&W Tek, Inc., Newark, Delaware), with an optical spectrum centered at 1310 nm and a bandwidth of 92 nm. Light is passed through an optical circulator (CIRC-3-31-P-BB-10-6:3port, Gould Fiber Optics, Millersville, Maryland) and into a 95/5 fiber-optic splitter (Gould Fiber Optics, Millersville, Maryland) that divides the light into a sample and reference arm. A 60 mm focal length achromatic lens in the sample arm focuses 4.75 mW of light to a 35  $\mu$ m spot (transverse resolution). The broad bandwidth source yields an axial resolution of 5.9  $\mu$ m in tissue. The depth-of-field of the lens (1.47 mm) closely matches the penetration depth of OCT in human breast tissue. Reflected light from the sample and reference arms is passed through polarization controllers (FPC-2, Fiber Control, Holmdel, New Jersey), coupled into an interferometer, spectrally dispersed by a diffraction grating (53004BK01-148R, Richardson Gratings, Newport Corporation, Rochester, New York, 1000 grooves / mm and blazed for 1310 nm), and focused onto an Indium Gallium Arsenide (InGaAs) line camera (SU1024LE-1.7T1-0500, Sensors Unlimited, Inc., Goodrich Corporation, Princeton, New Jersey) with a 150 mm singlet lens. With camera exposure times ranging from 24.4  $\mu$ s to 408.4  $\mu$ s, corresponding measured signal-to-noise ratios ranged from 96 dB to 116 dB. The imaging system acquires OCT images at a rate of ~5,000 axial scans per second or up to ~8-9 images per second (~600 axial scans / 10 mm). The sample is laterally scanned under the OCT beam using an automated translation stage. Data are collected using a high-speed data acquisition card with a 5 MHz sampling rate and 12-bit quantizer (PCI-6111E, National Instruments Corporation, Austin, Texas) in a dual Xeon processor (3.20 GHz) computer with 1 GB of RAM. Acquisition and processing time for an OCT image was ~5 sec / image. The OCT hardware and data acquisition are controlled by custom software written in LabVIEW and interfaced with a data processing sequence written in Matlab/C++. Due to the non-linear response from optical components, a cubic spline interpolation and resampling technique is implemented to compensate for aberrations (47). The data is assembled and displayed as a 2-D image.

### Imaging Protocol

Patients identified and recruited for this study had primary breast tumors (both *in-situ* and invasive carcinoma) in need of surgical resection by breast-conserving surgery, as determined by physicians at Carle Foundation Hospital and Carle Clinic Association, Urbana, Illinois, based on pre-operative radiological films, biopsy results, or other relevant diagnostic information. Patients undergoing mastectomy were excluded due to decreased likelihood of positive or close margins. No patients were excluded due to age or race. Patients were consented prior to surgery per protocols approved by institutional review boards at the University of Illinois at Urbana-Champaign and Carle Foundation Hospital. After surgical tissue resection but prior to margin assessment by the radiologist or pathologist, initial lumpectomy specimens were imaged in the operating room using OCT (Figure 2). A series of 10-20 parallel images were taken over a 1.0  $\times$  1.0 cm area. The researchers involved in image acquisition varied between imaging sessions and no information about the specimen was disclosed by the surgeon or staff during the sessions. Regions selected for OCT were based on suspicious visual or palpable findings as determined by the researchers, or were the entry-exit sites of localization guide wires. Following OCT imaging, one imaging site per specimen was marked with ink for correlation with histopathology, and the specimen was returned to surgical staff for standard processing and pathological margin assessment. In addition to histology sections acquired for diagnostic purposes as part of standard of care, sections co-registered with intraoperative OCT were acquired, stained, and correlated.

## OCT Image Processing & Evaluation Protocol

All OCT images were processed with the same standardization method and displayed on the same intensity scale (47). OCT images were initially evaluated in real-time by one of several researchers trained on the characteristic features found on OCT of breast tissue to ensure that the images were of sufficient quality for evaluation and to ensure that a subset of the images collected contained diagnostic features. Using criteria established from the training set, a single researcher during a single session, several months after data sets were acquired, evaluated all OCT images, identifying normal or abnormal features. Images with abnormal features were classified as positive, since the OCT imaging depth was within the 2 mm range commonly used to define close margins, and since the OCT image features were thought to be indicative of invasive or *in-situ* carcinoma. Since 10-20 OCT images were taken at each imaging site and correlated to a single histological section from that site, OCT margin assessment was made using the full set of available OCT images for each site.

## Histology Image Evaluation Protocol

Histology sections were acquired from marked areas imaged in the operating room with OCT. All tissue sections were stained with hematoxylin and eosin (H&E) and some were additionally immunohistochemically stained. Histology slides were digitized using a light microscope at 4X magnification and stitched together (Adobe Photoshop) to produce a single image. The compiled montage was oriented based on inked borders for later correlation to OCT images. H&E-stained histology images were classified by a board-certified pathologist as invasive carcinoma, *in-situ* carcinoma, other non-normal tissue, or normal tissue. Margins identified as carcinoma or other non-normal tissues were considered to be positive. The pathologist was blinded to the OCT images and results, giving an independent and unbiased assessment of the histology slide corresponding to the matching OCT image set.

## Results

### Patient Demographics

A total of 37 female patients were enrolled in the study. The training set consisted of 17 patients with a mean age of 62 (range from 44 to 82) and the study set consisted of 20 patients with a mean age of 66 (range from 41 to 84). Their final diagnoses, based on pathological findings and tumor margin assessments, included 15 cases of ductal carcinoma *in-situ*, 1 case of lobular carcinoma *in-situ*, 2 cases of infiltrating ductal carcinoma, 9 cases of invasive ductal carcinoma, 1 case of invasive papillary carcinoma, 2 cases of invasive mammary carcinoma, and 1 case of atypical ductal hyperplasia. The majority had more than one diagnosis classification associated with their histopathological assessment. An additional two patients in the training set and two in the study set were consented but subsequently excluded from the study and OCT imaging due to changes in surgery schedules or procedures.

### Training Data Set

An initial training data set of 78 OCT images from 17 patients (min = 2, max = 10, avg = 5 images / specimen) were used to establish standard imaging protocols, co-registration procedures, and image evaluation criteria of the surgical margins. Representative images shown in Figure 3 include normal adipose tissue (Fig. 3a), surgical artifacts of surface blood (Fig. 3b) and cauterized tissue (Fig. 3c), areas that appear duct-like in shape (Fig. 3d), and areas of highly scattering cells with spatially heterogeneous scattering intensity (Fig. 3d). These results were confirmed by gross visual findings or by histopathological analysis. Histopathological analysis reported DCIS involvement for the specimen imaged in Figure 3d. The training data set findings were used to establish the evaluation methodology and image feature criteria for identifying positive margins. These criteria included the presence or absence



of high-intensity scatterers, the location of these scatterers throughout the tissue, the heterogeneous/homogeneous spatial distribution of scattering intensity, and the morphological characteristics of these regions of interest. Surgical artifacts that could interfere with OCT evaluation such as surface blood and cauterized tissue appear as contiguous and highly scattering areas, remain localized to the immediate surface, and were quickly identified visually in the imaging field. In Figure 3b, a thin film ( $< 100 \mu\text{m}$ ) of homogeneous scatterers is representative of a bloody surface, while in Figure 3c, the cauterized tissue produced a highly scattering area which was observed within  $\sim 300 \mu\text{m}$  of the tissue surface. The region of interest in Figure 3d has both a high scattering intensity and a more heterogeneous composition indicative of cancerous tissue. In Figure 3d, the presence of highly scattering regions deep in the margin, instead of localized to the immediate surface, increases the likelihood that these features are intrinsic to the tissue architecture rather than a result of the surgical procedure.

### Study Data Set

OCT images with histological correlations from an additional 20 patients were used for the study set. A total of 210 OCT images were acquired from 20 lumpectomy specimens with an average of 10 OCT images per specimen. Using criteria established from the training set, the study set was evaluated and specimen margins were classified as positive or negative. A margin was considered positive if there was evidence of tumor cells or tissue either at the immediate surface, or within the imaging depth of OCT (1-2 mm). Eleven margins were identified as positive and 9 as negative under OCT image analysis. Analysis of corresponding H&E-stained histological sections yielded 9 true positives, 9 true negatives, 2 false positives, and 0 false negatives, giving a sensitivity of 100% and specificity of 82% (Table 1). Overall accuracy of OCT was 90% with a positive predictive value and a negative predictive value of 82% and 100%, respectively.

Three representative cases from the study set are presented in Figures 4 and 5. The first patient (female, age 66) was diagnosed with DCIS via ultrasound-guided core-needle biopsy with a 3.0 cm primary tumor. This case (Fig. 4) demonstrates OCT assessment of a negative tumor margin, which consists primarily of large lipid-filled adipocytes with interweaving microvasculature. The small dark highly-scattering point-like regions in the OCT image correspond to individual nuclei of adipocytes. Histological evaluation indicated that tumor cells were located more than 3 mm from the surface, confirming the OCT findings of a negative margin.

A second patient (female, age 60), diagnosed with invasive papillary carcinoma via ultrasound-guided core-needle biopsy, had a 0.8 cm primary tumor removed by lumpectomy. A third patient (female, age 51) was diagnosed with poorly differentiated infiltrating ductal carcinoma and high grade ductal carcinoma *in-situ* with a 2.3 cm primary tumor. Intraoperative OCT imaging of the margins (Fig. 5) revealed suspicious regions with increased and heterogeneous scattering within 1 mm of the inked surface (Fig. 5a, Patient #2, 60 F) and within 0.5 to 1.25 mm of the surface (Fig. 5c, Patient #3, 51 F). The matching H&E stained histology sections for the OCT images shown in Figures 5a and 5c are provided in Figures 5b and 5d, respectively, confirming the diagnostic features observed. These areas contained small and highly scattering cells contributing to the increased contrast, when compared to adjacent adipocytes. The increased scattering is from strong reflections from tightly packed cells, which provides the contrast observed in OCT. These results demonstrate distinct structural features identified with real-time intraoperative OCT on unstained tissue specimens that can be used to identify positive and negative margins without compromising the structural integrity of the specimens.

## Discussion

This study presents the first intraoperative demonstration of OCT as a real-time, high resolution imaging technique for the microscopic assessment of breast tumor margins. By providing subsurface imaging capabilities 1-2 mm deep with micron-scale resolution, OCT provides surgeons the ability to assess margin status in real-time, complementing current gross visual examination, potentially reducing the number of positive / close margins discovered postoperatively, and thereby reducing the need for additional surgical procedures. In the current standard-of-care, pathologists perform microscopic margin assessment within the 2mm range of the surface using FSA or PSA to determine the need for additional tissue removal.

OCT identified areas of homogeneous adipocytes, suspicious regions with highly scattering and tightly packed cells, and heterogeneous scattering patterns as some of the key features used to classify margins as negative or positive, as verified by histopathology. The large relative cell size difference easily separates the identification of adipocytes from tumor cells and stromal tissue. Increased nuclear density and changes in chromatin texture are believed to be responsible for high levels of scattering observed from cancer cells (41,42). At later tumor stages, observed characteristics change from open to filled ducts and lobules, and to heterogeneous tumor masses. Focal regions of scatterers embedded in adipose tissue were identified under OCT, indicative of smaller clusters of tumor cells. With more advanced cancer, areas of highly scattering tissue with irregular and heterogeneous patterns were identified. With an increased sampling rate of tumor margins with OCT, we expect to identify an increased number of positive surgical margins not otherwise grossly identifiable and likely missed due to limited sampling during standard histopathological analysis.

Surgical artifacts such as cauterized tissue and superficial blood are identified in OCT images as a contiguous layer of dark scatterers. These artifacts appear homogeneous in nature and are limited to the cut surface of the surgical margin rather than extending deep into the tissue. A relatively large pool of blood or cauterized tissue can limit the penetration depth of OCT due to high scattering. The imaging penetration depth with a bloody surface (Fig. 3b) is slightly diminished, compared to a cauterized surface (Fig. 3c) where penetration depth drops off sharply with little to no features observed beyond the cauterized tissue. Intravascular blood in small vessels and capillaries makes up a relatively small percentage of the tissue volume and has a minimal impact on the OCT penetration depth. In cases with residual surface blood, saline has been used to rapidly irrigate the surface to regain OCT imaging depth. OCT has been demonstrated for *in vivo* intravascular applications in humans, where an OCT imaging catheter is fully immersed in blood and imaging is performed following a saline flush (48). These surgical artifacts can be differentiated from intrinsic tissue properties, and can be quickly addressed without interfering with the ability of OCT to assess the margin. The presence of dyes such as methylene blue or lymphazurin which are used to map lymph drainage for sentinel and axillary lymph node dissections absorb in the spectral region below 700 nm (data not shown). Therefore, the presence of these dyes does not affect OCT imaging since our system operates in the spectral region around 1300 nm.

Recent advances in OCT technology have increased data acquisition speeds to 200,000 axial scans per second or greater (33). This would permit acquisition of 400 frames per second for a scan range of 10 mm and a lateral resolution of 35  $\mu\text{m}$ . For a 1  $\text{cm}^2$  area, imaging would be achieved in a few seconds while maintaining the full lateral resolution in both x and y directions. Novel computational algorithms such as Interferometric Synthetic Aperture Microscopy are being implemented for real-time OCT imaging, yielding spatially-invariant lateral resolution equivalent to that achieved at the focus of the beam (49). These combined advances offer the potential to vastly increase data acquisition rates and resolution without sacrificing the large scan area and real-time capabilities of OCT. The significant increase in data volume and limited

time to analyze and interpret image sets will increase the need for automated classification algorithms (40,44).

The differentiation of malignant (carcinoma) from benign (fibroadenoma) tumors is an ongoing research effort, as with many other biomedical imaging techniques. Stromal tissue, which makes up a larger percentage of breast tissue in younger patients, is primarily composed of connective tissue and favorably, is generally less scattering compared to tumor tissue (50). Studies have shown that the optical refractive index does not differ greatly between stromal and tumor tissue (46). Preliminary results from our laboratory have identified a promising combined method for distinguishing between the two tissue types by examining the power attenuation in the signal, the periodicity of the scattering profile, and the extracted refractive index information to aid in automated classification of OCT signals (40,45,46). Differentiation between benign fibrocystic changes versus malignant lesions will be important in further clinical studies. Cysts are expected to be readily distinguished due to their relatively large size, thin membranes, and low amount of scatterers within the cyst. Early morphological changes such as ductal hyperplasia or dysplasia, with increased cell density and nuclear-to-cytoplasm ratio, are likely to exhibit increased scattering, and ongoing work to improve resolution and to extract distinct image features may be necessary to distinguish these early changes.

This report demonstrates the potential of real-time intraoperative OCT for margin assessment from resected breast lumpectomy specimens. OCT acquires images in the same physical range as that used in histology to classify surgical margins as positive, close (<2mm), or negative. The development of faster scanning handheld probes will allow surgeons to quickly scan the *in-situ* tumor cavity wall in addition to the lumpectomy specimen margin, providing guidance on tissue removal. *In-situ* OCT imaging would effectively double the sampling depth by evaluating depths up to 2 mm on the specimen and on the cavity wall. Further studies with even higher resolution, comprehensive volumetric imaging, and automated tissue type classification are expected to reveal additional unique features that can be used to further improve the identification of positive and negative margins intraoperatively with OCT. Intraoperative identification of positive margins will decrease the need for additional surgical procedures and the rate of local recurrence in breast cancer patients.

## Acknowledgments

The authors thank the physicians, staff, and administration at Carle Foundation Hospital and Carle Clinic Association for their research support. The authors thank Dr. Daniel L. Marks for his technical discussions and contributions toward this project. This research was supported in part by the National Institutes of Health (R01 EB005221, S.A.B.), the University of Illinois at Urbana-Champaign and University of Illinois at Chicago Intercampus Research Initiative in Biotechnology (S.A.B.), the Grainger Foundation (S.A.B.), and Carle Foundation Hospital (S.A.B.). F.T.N. was supported in part by a grant from the U.S. Department of Defense (BC073292).<sup>1</sup>

## References

1. Cancer Facts & Figures 2009. American Cancer Society; Atlanta: 2009.
2. Taghian A, Mohiuddin M, Jagsi R, Goldberg S, Ceilley E, Powell S. Current perceptions regarding surgical margin status after breast-conserving therapy: results of a survey. *Ann Surg* 2005;241:629–39. [PubMed: 15798465]
3. Dillon MF, Hill AD, Quinn CM, McDermott EW, O'Higgins N. A pathologic assessment of adequate margin status in breast-conserving therapy. *Ann Surg Oncol* 2006;13:333–9. [PubMed: 16474911]
4. Luini A, Rososchansky J, Gatti G, et al. The surgical margin status after breast-conserving surgery: discussion of an open issue. *Breast Cancer Res Treat*. 2008

<sup>1</sup>Additional information can be found at <http://biophotonics.illinois.edu>.



5. Aziz D, Rawlinson E, Narod SA, et al. The role of reexcision for positive margins in optimizing local disease control after breast-conserving surgery for cancer. *Breast J* 2006;12:331–7. [PubMed: 16848842]
6. Cefaro GA, Genovesi D, Marchese R, et al. Predictors of local recurrence after conservative surgery and whole-breast irradiation. *Breast Cancer Res Treat* 2006;98:329–35. [PubMed: 16555125]
7. Cellini C, Hollenbeck ST, Christos P, et al. Factors associated with residual breast cancer after re-excision for close or positive margins. *Ann Surg Oncol* 2004;11:915–20. [PubMed: 15383425]
8. Connolly JL, Boyages J, Nixon AJ, et al. Predictors of breast recurrence after conservative surgery and radiation therapy for invasive breast cancer. *Mod Pathol* 1998;11:134–9. [PubMed: 9504684]
9. Dillon MF, Mc Dermott EW, O'Doherty A, Quinn CM, Hill AD, O'Higgins N. Factors affecting successful breast conservation for ductal carcinoma *in situ*. *Ann Surg Oncol* 2007;14:1618–28. [PubMed: 17443388]
10. Huston TL, Pigalarga R, Osborne MP, Tousimis E. The influence of additional surgical margins on the total specimen volume excised and the reoperative rate after breast-conserving surgery. *Am J Surg* 2006;192:509–12. [PubMed: 16978962]
11. McIntosh A, Freedman G, Eisenberg D, Anderson P. Recurrence rates and analysis of close or positive margins in patients treated without re-excision before radiation for breast cancer. *Am J Clin Oncol* 2007;30:146–51. [PubMed: 17414463]
12. van der Velden, AP Schouten; Van de Vrande, SL.; Boetes, C.; Bult, P.; Wobbes, T. Residual disease after re-excision for tumour-positive surgical margins in both ductal carcinoma in situ and invasive carcinoma of the breast: The effect of time. *J Surg Oncol* 2007;96:569–74. [PubMed: 17680635]
13. Scopa CD, Aroukatos P, Tsamandas AC, Aletra C. Evaluation of margin status in lumpectomy specimens and residual breast carcinoma. *Breast J* 2006;12:150–3. [PubMed: 16509840]
14. Smitt MC, Nowels KW, Zdeblick MJ, et al. The importance of the lumpectomy surgical margin status in long-term results of breast conservation. *Cancer* 1995;76:259–67. [PubMed: 8625101]
15. Swanson GP, Rynearson K, Symmonds R. Significance of margins of excision on breast cancer recurrence. *Am J Clin Oncol* 2002;25:438–41. [PubMed: 12393979]
16. Zavagno G, Goldin E, Mencarelli R, et al. Role of resection margins in patients treated with breast conservation surgery. *Cancer* 2008;112:1923–31. [PubMed: 18327818]
17. Cefaro GA, Genovesi D, Marchese R, et al. The effect of delaying adjuvant radiation treatment after conservative surgery for early breast cancer. *Breast J* 2007;13:575–80. [PubMed: 17983399]
18. van der Velden AP, Peeters PH, Koot VC, Hennipman A. Local Recurrences After Conservative Treatment of Ductal Carcinoma-In-Situ of the Breast Without Radiotherapy: The Effect of Age. *Ann Surg Oncol*. 2006
19. Olson TP, Harter J, Munoz A, Mahvi DM, Breslin T. Frozen section analysis for intraoperative margin assessment during breast-conserving surgery results in low rates of re-excision and local recurrence. *Ann Surg Oncol* 2007;14:2953–60. [PubMed: 17674109]
20. McLaughlin SA, Ochoa-Frongia LM, Patil SM, Cody HS 3rd, Sclafani LM. Influence of frozen-section analysis of sentinel lymph node and lumpectomy margin status on reoperation rates in patients undergoing breast-conservation therapy. *J Am Coll Surg* 2008;206:76–82. [PubMed: 18155571]
21. Valdes EK, Boolbol SK, Cohen JM, Feldman SM. Intra-operative touch preparation cytology; does it have a role in re-excision lumpectomy? *Ann Surg Oncol* 2007;14:1045–50. [PubMed: 17206481]
22. Goldfeder S, Davis D, Cullinan J. Breast specimen radiography: can it predict margin status of excised breast carcinoma? *Acad Radiol* 2006;13:1453–9. [PubMed: 17138112]
23. Erguvan-Dogan B, Whitman GJ, Nguyen VA, et al. Specimen radiography in confirmation of MRI-guided needle localization and surgical excision of breast lesions. *AJR Am J Roentgenol* 2006;187:339–44. [PubMed: 16861535]
24. Karni T, Pappo I, Sandbank J, et al. A device for real-time, intraoperative margin assessment in breast-conservation surgery. *Am J Surg* 2007;194:467–73. [PubMed: 17826057]
25. Haka AS, Volynskaya Z, Gardecki JA, et al. *In vivo* margin assessment during partial mastectomy breast surgery using Raman spectroscopy. *Cancer Res* 2006;66:3317–22. [PubMed: 16540686]
26. Boppart SA, Bouma BE, Pitris C, Southern JF, Brezinski ME, Fujimoto JG. *In vivo* cellular optical coherence tomography imaging. *Nat Med* 1998;4:861–5. [PubMed: 9662382]

27. Boppart SA, Bouma BE, Pitris C, et al. Intraoperative assessment of microsurgery with three-dimensional optical coherence tomography. *Radiology* 1998;208:81–6. [PubMed: 9646796]
28. Boppart SA, Deutsch TF, Rattner DW. Optical imaging technology in minimally invasive surgery. Current status and future directions. *Surg Endosc* 1999;13:718–22. [PubMed: 10384083]
29. Boppart SA, Luo W, Marks DL, Singletary KW. Optical coherence tomography: feasibility for basic research and image-guided surgery of breast cancer. *Breast Cancer Res Treat* 2004;84:85–97. [PubMed: 14999139]
30. Bouma, BE.; Tearney, GJ. *Handbook of optical coherence tomography*. Marcel Dekker; New York: 2002.
31. Fujimoto JG, Pitris C, Boppart SA, Brezinski ME. Optical coherence tomography: an emerging technology for biomedical imaging and optical biopsy. *Neoplasia* 2000;2:9–25. [PubMed: 10933065]
32. Huang D, Swanson EA, Lin CP, et al. Optical coherence tomography. *Science* 1991;254:1178–81. [PubMed: 1957169]
33. Huber R, Adler DC, Fujimoto JG. Buffered Fourier domain mode locking: Unidirectional swept laser sources for optical coherence tomography imaging at 370,000 lines/s. *Opt Lett* 2006;31:2975–7. [PubMed: 17001371]
34. de Boer JF, Milner TE, van Gemert MJ, Nelson JS. Two-dimensional birefringence imaging in biological tissue by polarization-sensitive optical coherence tomography. *Opt Lett* 1997;22:934–6. [PubMed: 18185711]
35. Oldenburg AL, Crecea V, Rinne SA, Boppart SA. Phase-resolved magnetomotive OCT for imaging nanomolar concentrations of magnetic nanoparticles in tissues. *Opt Express* 2008;16:11525–39. [PubMed: 18648474]
36. Xu C, Vinegoni C, Ralston TS, Luo W, Tan W, Boppart SA. Spectroscopic spectral-domain optical coherence microscopy. *Opt Lett* 2006;31:1079–81. [PubMed: 16625909]
37. Lee TM, Oldenburg AL, Sitafalwalla S, et al. Engineered microsphere contrast agents for optical coherence tomography. *Opt Lett* 2003;28:1546–8. [PubMed: 12956374]
38. Yang C. Molecular contrast optical coherence tomography: a review. *Photochem Photobiol* 2005;81:215–37. [PubMed: 15588122]
39. Zysk AM, Nguyen FT, Oldenburg AL, Marks DL, Boppart SA. Optical coherence tomography: a review of clinical development from bench to bedside. *J Biomed Opt* 2007;12:051403. [PubMed: 17994864]
40. Zysk AM, Boppart SA. Computational methods for analysis of human breast tumor tissue in optical coherence tomography images. *J Biomed Opt* 2006;11:054015. [PubMed: 17092164]
41. Arifler D, Guillaud M, Carraro A, Malpica A, Follen M, Richards-Kortum R. Light scattering from normal and dysplastic cervical cells at different epithelial depths: finite-difference time-domain modeling with a perfectly matched layer boundary condition. *J Biomed Opt* 2003;8:484–94. [PubMed: 12880355]
42. Drezek R, Guillaud M, Collier T, et al. Light scattering from cervical cells throughout neoplastic progression: influence of nuclear morphology, DNA content, and chromatin texture. *J Biomed Opt* 2003;8:7–16. [PubMed: 12542374]
43. Hsiung PL, Phatak DR, Chen Y, Aguirre AD, Fujimoto JG, Connolly JL. Benign and malignant lesions in the human breast depicted with ultrahigh resolution and three-dimensional optical coherence tomography. *Radiology* 2007;244:865–74. [PubMed: 17630358]
44. Goldberg BD, Iftimia NV, Bressner JE, et al. Automated algorithm for differentiation of human breast tissue using low coherence interferometry for fine needle aspiration biopsy guidance. *J Biomed Opt* 2008;13:014014. [PubMed: 18315372]
45. Zysk AM, Adie SG, Armstrong JJ, et al. Needle-based refractive index measurement using low-coherence interferometry. *Opt Lett* 2007;32:385–7. [PubMed: 17356661]
46. Zysk AM, Chaney EJ, Boppart SA. Refractive index of carcinogen-induced rat mammary tumours. *Phys Med Biol* 2006;51:2165–77. [PubMed: 16625033]
47. Nguyen, FT.; Zysk, AM.; Kotynek, JG., et al. Portable real-time optical coherence tomography system for intraoperative imaging and staging of breast cancer. In: Vo-Dinh, WSG Tuan; Benaron, David A.; Cohn, Gerald E.; Raghavachari, Ramesh, editors. *SPIE - Photonics West BiOS - Advanced Biomedical and Clinical Diagnostic Systems V*. San Jose, CA: Feb 6. 2007 20072007

48. Bouma BE, Tearney GJ, Yabushita H, et al. Evaluation of intracoronary stenting by intravascular optical coherence tomography. *Heart* 2003;89:317–20. [PubMed: 12591841]
49. Ralston TS, Marks DL, Carney P Scott, Boppart SA. Interferometric synthetic aperture microscopy. *Nat Phys* 2007;3:129–34.
50. Abramson RG, Mavi A, Cermik T, et al. Age-related structural and functional changes in the breast: multimodality correlation with digital mammography, computed tomography, magnetic resonance imaging, and positron emission tomography. *Seminars in nuclear medicine* 2007;37:146–53. [PubMed: 17418148]

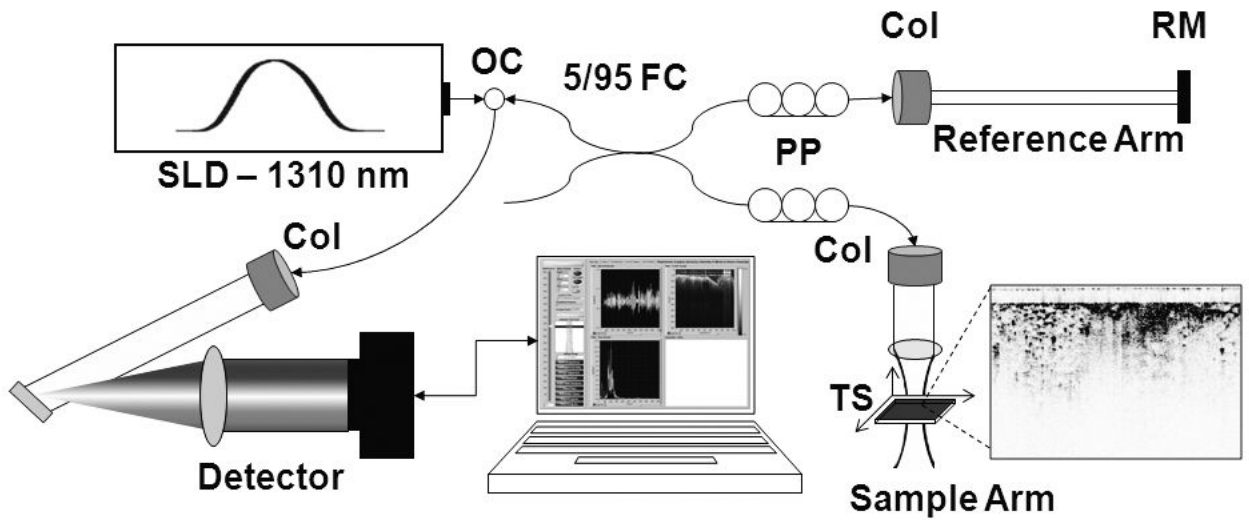


**Figure 1.** Clinical spectral-domain optical coherence tomography system schematic. Light from a SLD ( $\lambda=1310$  nm) is directed into an optical circulator (OC) and to a fiber coupler (FC) which splits 5% of the light to a reference arm mirror (RM) and 95% of the light to a sample arm containing focusing optics and an automated x-y translation stage (TS). Light is collimated through fiber collimators (Col). Reflected light from each arm is coupled through polarization paddles (PP), interfered within the fiber coupler, and spectrally dispersed onto a line camera.

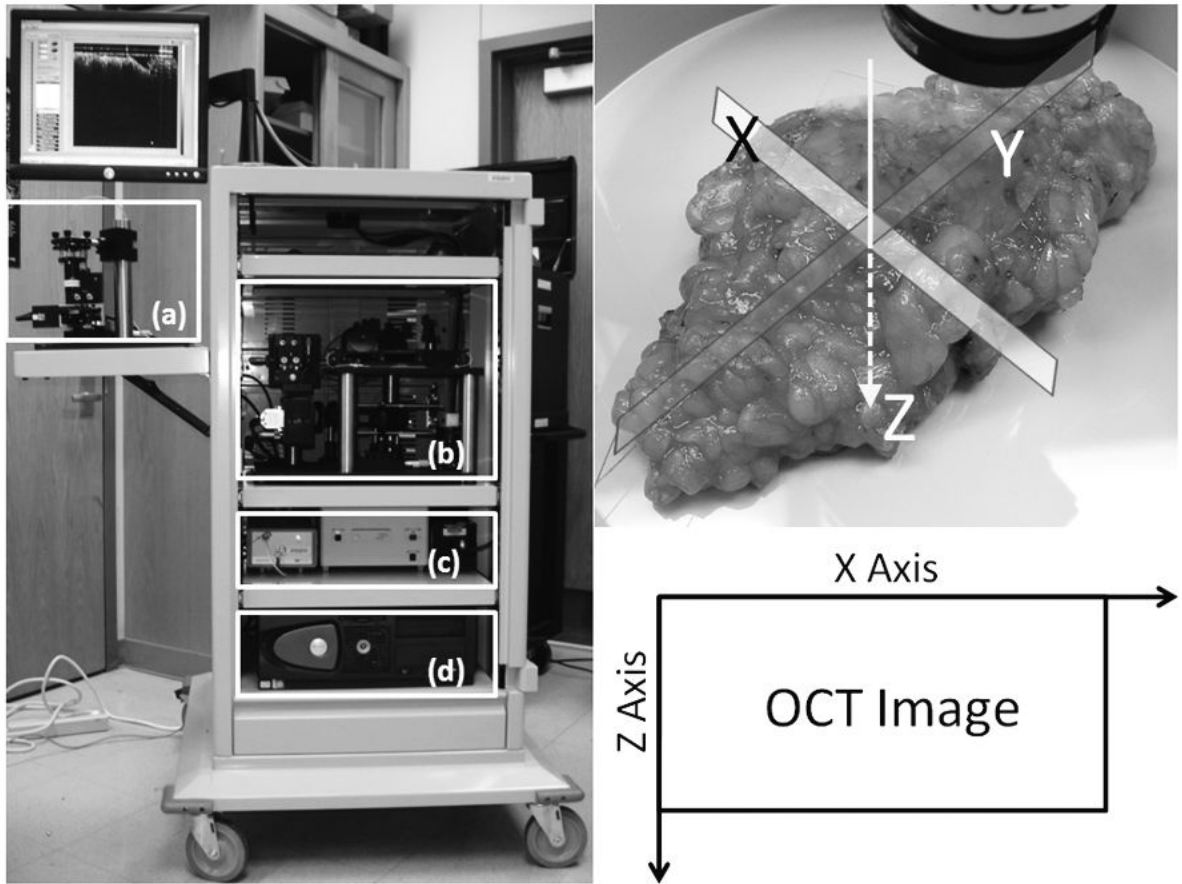


**Figure 2.** Photograph of the clinical SD-OCT system housed in a standard endoscopy cart (left). This system is portable for use in various surgical suites. Resected surgical specimens are placed on the sample-arm stage (a). The detector and reference arm (b) are located within the cart, along with the light source and hardware controllers (c) and computer (d). OCT images (shown in later figures) represent 2-D cross-sectional planes (x-z) oriented perpendicular to the tissue surface (right). Multiple OCT images can be acquired by stepping the beam in the y direction.



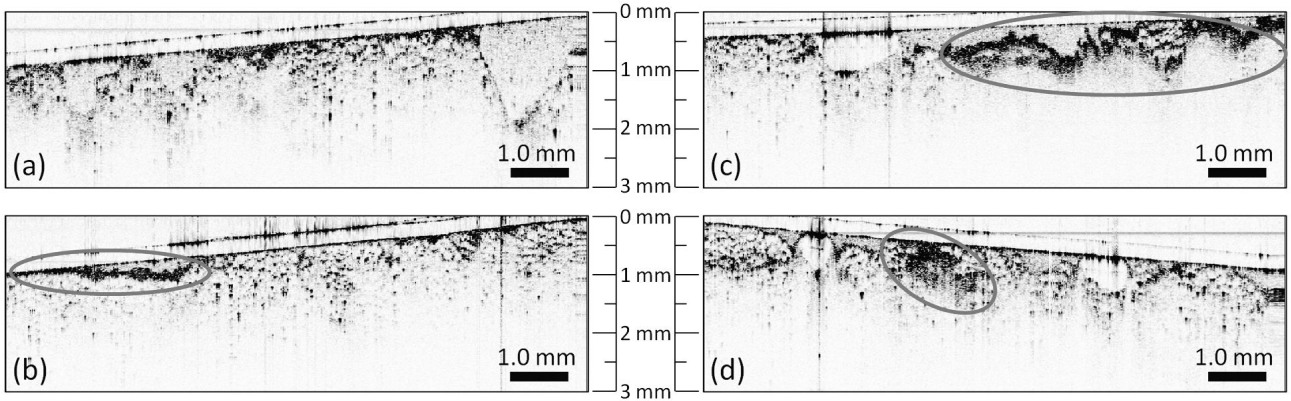


**Figure 3.** Representative OCT images of surgical margins from lumpectomy specimens acquired for the training set. Images of normal tissue (a) were identified by the homogenous pattern of large adipose cells. Readily identified surgical artifacts include blood (b) which appears as a thin film of scatterers, and cauterized tissue (c) which has a patch-like appearance. Images of positive margins (d) containing tumor cells and tissue included a highly scattering area that was more heterogeneous and disruptive of the surrounding architecture.

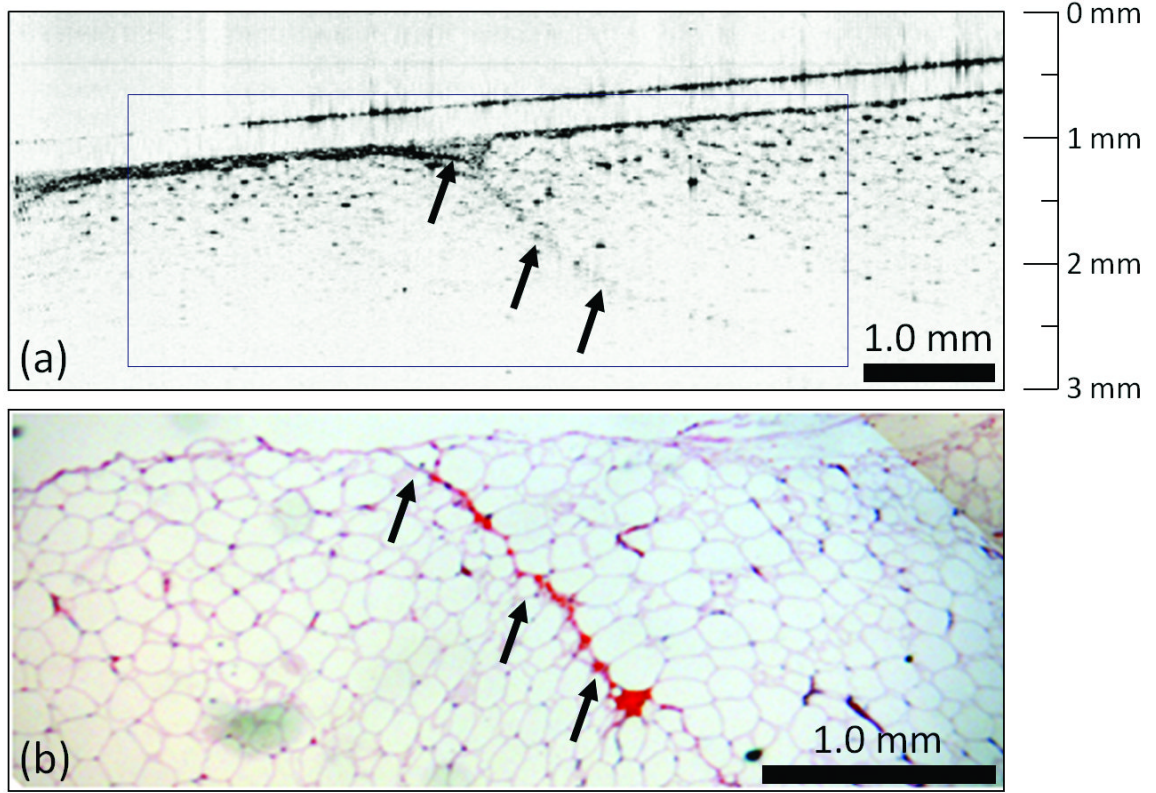


**Figure 4.** Negative tumor margin. OCT (a) and corresponding H&E-stained histology (b) of normal breast tissue near the surface of a lumpectomy specimen. The large adipose cells with point-like scattering nuclei dominate the OCT image, which also contains a region of the microvasculature (arrows). Features found in the real-time intraoperative OCT image correspond well to those identified in the post-surgical paraffin-embedded histology section.

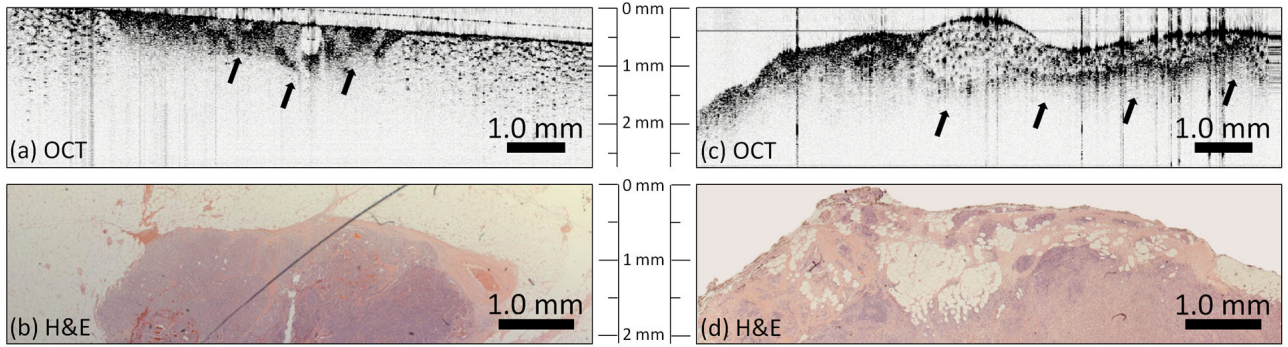


**Figure 5.** Positive tumor margins. OCT images (a, c) show a distinct heterogeneously-scattering region (arrows) with small, highly scattering foci indicative of collections of tumor cells. These features clearly extend to the surface of the specimen (to the surgical margin) in (a) and the left side of (c), but also are evident below adipose tissue in (c). The OCT image in (a) was acquired with a coverslip over the surface to reduce backreflection artifacts, which appear as vertical lines in (c). Corresponding H&E-stained histology (b, d) images show corresponding features, confirming the presence of these positive margins.

**Table 1**

Intraoperative Tumor Margin Assessment (OCT vs. Histopathology).

	Histology (Positive)	Histology (Negative)	Total	
OCT (Positive)	9 (TP)	2 (FP)	11	PPV = 82%
OCT (Negative)	0 (FN)	9 (TN)	9	NPV = 100%
<b>Total</b>	9	11	20	
	Sensitivity = 100%		Specificity = 82%	